Environ Fluid Mech
DOI 10.1007/s10652-016-9501-0

ORIGINAL ARTICLE

Lock-exchange gravity currents over rough bottoms

C. Cenedese[1] · R. Nokes[2] · J. Hyatt[3]

Received: 16 July 2016 / Accepted: 12 December 2016

Abstract In nature, density driven currents often flow over or within a bottom roughness: a sea breeze encountering tall buildings, a shallow flow encountering aquatic vegetation, or a dense oceanic current flowing over a rough bottom. Laboratory experiments investigating the mechanisms by which bottom roughness enhances or inhibits entrainment and dilution in a lock-exchange dense gravity current have been conducted. The bottom roughness has been idealized by an array of vertical, rigid cylinders. Both spacing (sparse vs. dense configuration) and height of the roughness elements compared with the height of the current have been varied. Two-dimensional density fields have been obtained. Experimental results suggest that enhancement of the entrainment/dilution of the current can occur due to two different mechanisms. For a sparse configuration, the dense current propagates between the cylinders and the entrainment is enhanced by the vortices generated in the wake of the cylindrical obstacles. For a dense configuration, the dense current rides on top of the cylinders and the dilution is enhanced by the onset of convective instability between the dense current above the cylinders and the ambient lighter water between the cylinders. For low values of the ratio of the cylinder to lock height λ the dense current behavior approaches that of a current over a smooth bottom, while the largest deviations from the smooth bottom case are observed for large values of λ.

✉ C. Cenedese
ccenedese@whoi.edu

R. Nokes
roger.nokes@canterbury.ac.nz

J. Hyatt
jhyatt@maritime.edu

[1] Department of Physical Oceanography, Woods Hole Oceanographic Institution, MS#21, 360 Woods Hole Road, Woods Hole, MA 02543, USA

[2] Department of Civil and Natural Resources Engineering, University of Canterbury, Christchurch 8140, New Zealand

[3] Department of Science and Mathematics, Massachusetts Maritime Academy, Buzzards Bay, MA 02532, USA

Published online: 26 December 2016

Keywords Gravity currents · Roughness · Mixing

1 Introduction

Gravity currents are ubiquitous in the environment and occur in the presence of horizontal density gradients in a fluid under the action of a gravitational field. The density gradients can be due to temperature differences with the generation, for example, of sea breezes; differences in particulate suspension with the generation, for example, of volcanic pyroclastic flows in the atmosphere and turbidity currents in the ocean; differences in solute concentration which may generate, for example, oceanographic overflows. [27] provides an excellent overview of the dynamics of these currents and their appearance in natural settings.

Gravity currents propagating over a smooth horizontal bottom have been extensively investigated using the lock-exchange configuration where two motionless fluids of different densities are separated by a vertical lock. After the lock is removed, the horizontal density gradient generates a denser current propagating along the bottom and a lighter current propagating in the opposite direction along the top surface. Numerous experimental (e.g. [1, 9, 12, 25, 26]), theoretical (e.g. [31]), and numerical (e.g. [5, 16, 22, 24]) studies have been conducted to investigate different aspects of gravity currents.

Recent studies (e.g. [6, 10, 14, 32]) focused primarily on the entrainment occurring in the shear region at the top of the dense current. In thick currents, where the height is much larger than the bottom boundary layer thickness, mixing occurring in the bottom low Richardson number region contributes to the homogenization of the densest water mass, while most of the entrainment is confined to the top of the current. However, for dense currents where the height is comparable to the bottom boundary layer thickness, bottom friction and roughness elements are likely to influence entrainment which may be due to a combination of shear-driven turbulence at the top of the current and turbulent eddies generated by the bottom roughness.

A research area of increasing interest is the interaction of gravity currents with bottom roughness. Several studies have focused on flow through forest canopies (e.g. [2, 8]) and urban canopies (e.g. [4, 13]). With the aim of understanding fluid flow through aquatic canopies, several studies have investigated a homogeneous fluid flow through vertical cylinders, both flexible and rigid, which occupy a fraction or the entire water depth, and focused mainly on the enhanced drag and dispersion due to bottom roughness. An excellent review of these studies is given in [18]. A non-dimensional measure of the roughness density is the frontal area per bed area. Consider four vertical cylinders of diameter d located at the vertices of a square of side ΔS and extending for a height h. In the volume of base ΔS^2, the frontal area of the cylinders is dh while the bed area is ΔS^2. Hence, the frontal area per bed area is $ah = dh/\Delta S^2$, where $a = d/\Delta S^2$ and ΔS is, in general, the average spacing between the elements. For submerged roughness, there are two different regimes depending on the relative importance of the bottom drag compared to the roughness drag. For $ah \ll 0.1$ the roughness drag is small compared to the bottom drag and the velocity profile follows a logarithmic turbulent boundary-layer profile. If the roughness drag is large compared to the bottom drag, i.e. $ah \gg 0.1$, a region of shear is generated near the top of the roughness elements. Canopies, made of relatively thin and tall elements, were observed to generate two distinct scales of turbulence: stem-scale turbulence

generated within the canopy, and canopy-scale turbulence generated by the flow shear instability at the top of the canopy [18].

Relatively few studies have investigated the flow of a gravity current through or over a rough bottom. Laboratory studies investigated the exchange flow, mean drag and propagation velocity of a dense current moving through regular and random arrays of vertical rigid cylinders extending throughout the entire water depth (e.g. [28–30, 33]). Numerical studies focusing again on the drag force acting on the gravity current and front velocity, investigated gravity currents propagating through a porous medium generated by a staggered array of rigid horizontal cylinders aligned with their axes perpendicular to the flow direction [23]. The only laboratory study with a configuration similar to the present one, investigated the dynamics of a surface buoyant gravity current propagating through a suspended canopy represented by an array of vertical circular cylinders. The focus was to collect velocity measurements to understand the exchange flow through the canopy [34].

Bottom roughness has been observed to inhibit the formation and collapsing mechanism of Kelvin–Helmholtz instabilities at the interface [17], hence affecting the entrainment into the current. [19, 20], and [15] investigated the dynamics of a dense current flowing over irregular rough beds (generated using sediments of different diameter) and observed that the dense current slows down and the entrainment is enhanced (with the exception of the highest roughness) with increasing roughness (i.e., increasing sediment diameter).

The above fundamental studies of turbulent flows over rough surfaces have clearly revealed that the roughness shape, distribution, and the spacing between roughness elements significantly alter the wall shear (i.e., the frictional velocity) and also the mean velocity, and consequently the Froude number, of the current. Hence, the presence of bottom roughness not only may introduce an additional mechanism for entrainment, but can also modify the entrainment occurring at the upper boundary of the dense current. The current paper investigates the dynamics of lock-exchange gravity currents over rough bottoms with different spacing between the roughness elements and different height of the elements. The novel aspect of the present study is to identify and classify the different dynamical regimes the current undergoes as the non-dimensional parameters regulating the bottom roughness and the initial condition are varied over a wide range of values, and to investigate the entrainment and dilution of the current using novel density measurements.

The paper is organized as follows: the methods are described in Sect. 2 and the non-dimensional parameters are introduced in Sect. 3. The two different regimes observed for lock-exchange gravity currents moving over sparse and dense rough bottoms are described in Sect. 4 and the current dilution in these two regimes is discussed in Sect. 5. The classification of the experiments based on the speed of the current propagating on top of the cylinders relative to that of the fluid between the cylinders is given in Sect. 6 and the influence of the rough bottom on the front speed is discussed in Sect. 7. Finally, our conclusions are given in Sect. 8.

2 Methods

2.1 Experimental set up

Experiments were conducted in a tank ($L_T = 620$ cm, $H_T = 50$ cm, $W_T = 25$ cm) with a flat bottom in which a dense gravity current was generated using the classic lock-exchange configuration. A stainless steel gate, sealed by plastic foam, was positioned 100 cm from

the right hand end of the tank forming what hereafter we will call the 'lock' region (Fig. 1). The fluid in the lock comprised a 4 g/l salt solution with density $\rho_d \approx 1.0014$ g/cm^3 while the fluid in the rest of the tank was a solution of clear denatured ethanol and water (14 ml ethanol per 114 ml ethanol-water mixture) with a density $\rho_0 \approx 0.9963$ g/cm^3 selected to match the refractive index $n = 1.3336$ of the salt solution. All waters were stored at room temperature. The solution of water and ethanol was mixed vigorously with a pump for at least 30 min and its density was measured at different locations within the tank to assure that the fluid was homogeneous before the experiment was initiated. The density difference $\Delta\rho = \rho_d - \rho_0$ produced a reduced gravity $g' = g\Delta\rho/\rho \approx 5$ cm/s^2 for all experiments. The densities were measured with an Anton Paar DMA5000 density meter. The denser fluid in the lock occupied the total water depth (Fig. 1) which assumed values $H = 10$, 15, 20, 27, or 35 cm.

The bottom roughness was idealized by an array of vertical cylinders located in the lighter fluid region for 300 cm beyond the gate (Fig. 1). The cylinders were made of rigid plastic with a diameter of $d = 2$ cm and their height varied between different experiments and was either $h = 1$, 2, or 5 cm. The cylinders were screwed into an aluminum base plate and could be removed or added to change the distance ΔS between their centers (Fig. 1). This distance took values of $\Delta S = 3.2$ cm in what we will call hereafter the 'dense' configuration and $\Delta S = 6.4$ cm in the 'sparse' configuration. A total of 30 experiments were conducted with bottom roughness present, and 5 with a smooth bottom.

2.2 Density measurements

Two-dimensional, cross-tank averaged, density fields were obtained using a Light Attenuation (LA) technique [7] with *Streams*, a software tool designed to support the analysis of images obtained from experimental fluid flows [21]. The images were recorded using a JAI BB141GE video camera with a zoom lens operating at 30.13 Hz. The 1392x1040 pixel images were transferred directly to a fast hard drive on a PC during capture. The field of

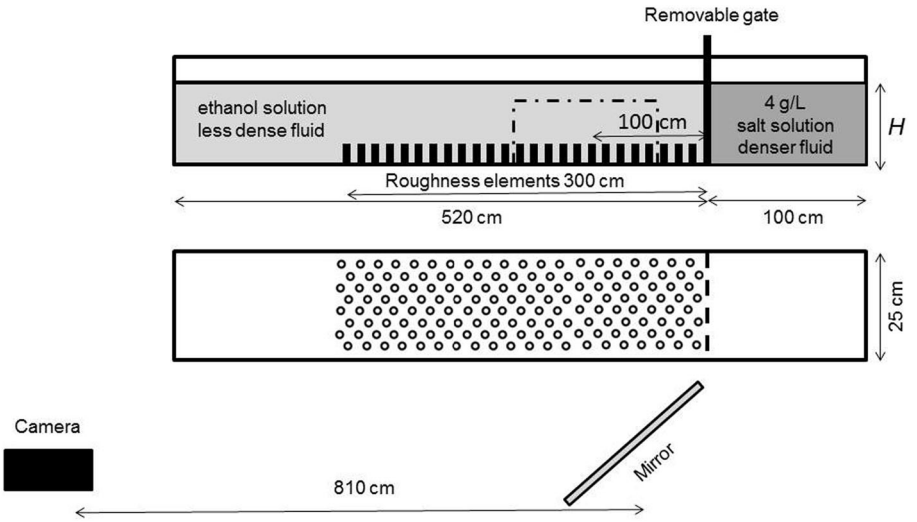

Fig. 1 Schematic of the experimental set up. *Top* elevation view. *Bottom* plan view. *Dashed-dotted lines* illustrate the location of the camera field of view. Not to scale

view of the camera was centered 100 cm downstream of the lock and was 50 cm wide. The camera viewed the flow through an angled mirror to extend the light path and minimize parallax (Fig. 1).

In order to measure density using LA, the flow was illuminated from the rear by a bank of fluorescent bulbs. Care was taken to ensure consistent lighting throughout the calibration and experiments. A reserve of concentrated dyed red salty solution was made and the tank and lighting were calibrated by measuring density and light attenuation at 8 different concentrations. The concentrate was then used to create the denser fluid in the lock. The experimental densities were calculated using a pixel by pixel calibration curve based on Beer's Law and the ratio of the average of blue and green/red intensity. The error in the density measurements was always less than 5% and generally much lower than that.

The final output from the LA analysis process was a non-dimensional, cross tank averaged, 2D concentration field translated into the frame of reference moving with the gravity current front. In order to achieve the latter it was necessary to assume that the current front traveled at a constant speed, and that in this moving frame of reference the flow characteristics were statistically stationary. Measurements of the front speed indicated that the first of these assumptions was reasonable for the duration of our experiments - typically 33 s. Furthermore, in order to obtain smooth density fields in which the turbulent fluctuations are suitably averaged, the data are also presented as a time average over the acquisition period, as shown in Fig. 2. The flow is turbulent but approximately in steady state, i.e. in the frame of reference moving with the gravity current front the density at each location is fluctuating about a steady mean value, hence the time averaging process only averages the turbulent fluctuations and does not smooth out any other information. However, caution must be taken when averaging in the region within the roughness elements, since only data within the fluid must be averaged. In the camera field of view, the gap between the cylinders in the dense and sparse configuration was 0.8 and 3.5 cm, respectively, as shown in Fig. 3. The fraction of images with data available to be averaged

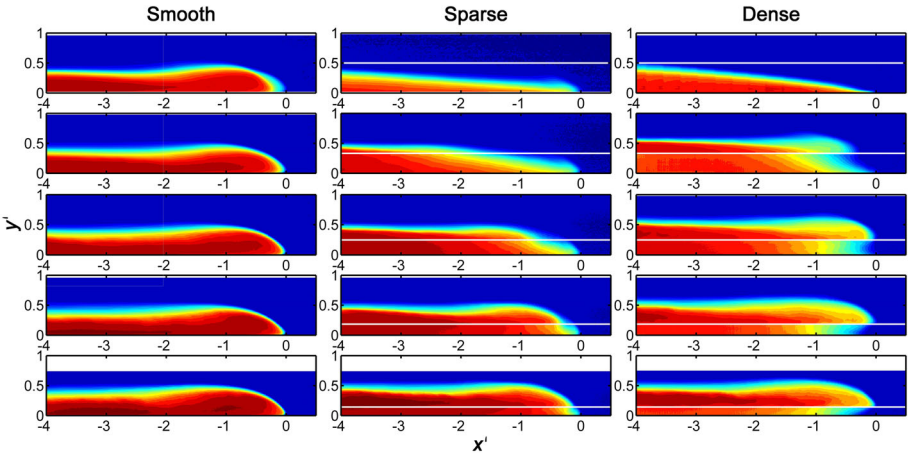

Fig. 2 Time averaged, non-dimensional density field for a gravity current propagating over a (*left column*) smooth bottom, and a (*center column*) sparse and (*right column*) dense rough bottom. For the sparse and dense configurations $\alpha = 2.5$. *Different rows* represent experiments with different lock height and the values of λ for the sparse and dense configurations, from *top* to *bottom* row, are: 0.50, 0.33, 0.25, 0.18 and 0.14. The *white line* indicates the height of the roughness elements. *Blue* represents ambient light fluid and *red* undiluted lock dense fluid

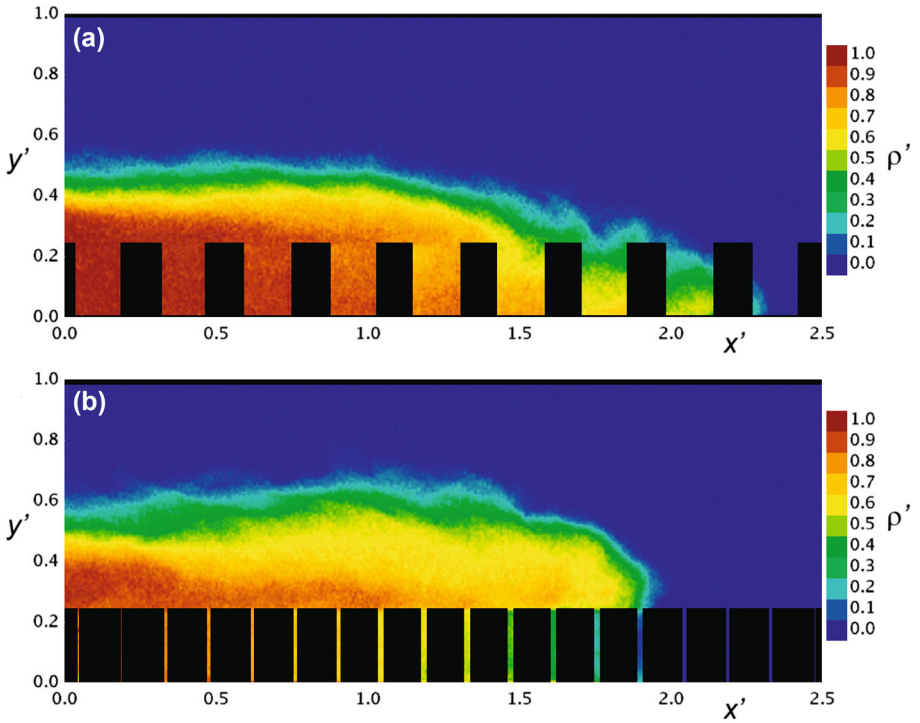

Fig. 3 Instantaneous non-dimensional density field for a gravity current propagating into a **a** sparse and **b** dense array of *cylinders* representing the bottom roughness. The non-dimensional parameters for **a** are: $\sigma = 0.09$, $\mu = 0.31$, $\alpha = 2.5$, $\lambda = 0.25$, $Fr = 0.35$ and $Re = 7165$; and for **b** are: $\sigma = 0.35$, $\mu = 0.62$, $\alpha = 2.5$, $\lambda = 0.25$, $Fr = 0.28$ and $Re = 5600$

within these gaps is given by the ratio of the gap width to the sum of the cylinder diameter and gap width, i.e. 0.28 and 0.64 for the dense and sparse configuration, respectively. Hence, while above the roughness elements all of the images were averaged in time, for each pixel within the roughness elements only 28% (dense) and 64% (sparse) of the images was available for the time averaging. The LA analysis intrinsically averages the data in the across flow direction and, while the averaged data in the dense configuration are the least accurate, the smoothness of the density fields within the roughness elements (Fig. 2) indicates that the turbulent fluctuations have been adequately averaged.

The variables were non-dimensionalised as follows:

$$x' = \frac{x}{H} \qquad \text{and} \qquad y' = \frac{y}{H}, \tag{1}$$

and

$$\rho' = \frac{\rho - \rho_0}{\rho_d - \rho_0}, \tag{2}$$

where x and y are the horizontal and vertical coordinates, respectively, with the origin of y' being the bottom of the tank, the origin of x' selected to be the furthest downstream location of the $\rho' = 0.1$ contour, and with the co-ordinate axis x' oriented to increase in the downstream direction.

3 Dimensionless parameters

The bottom roughness is characterized by three dimensionless parameters. The elevation density, μ, defined by

$$\mu = \frac{A_E}{A_{TE}} = \frac{d}{\Delta S}, \tag{3}$$

where A_E is the area of the field covered by the cylinders in elevation as seen by the advancing current and A_{TE} is the total area of the field in elevation (measured to the top of the cylinders); σ, the plan density, defined by

$$\sigma = \frac{A_P}{A_{TP}} = \frac{\pi}{4}\gamma\mu^2, \tag{4}$$

where A_P is the area of the base covered by the cylinders in plan, A_{TP} is the total area of the base in plan and $\gamma = \frac{2}{\sqrt{3}}$ for our configuration (Fig. 1); and α, the aspect ratio of the roughness elements, defined by

$$\alpha = \frac{h}{d}. \tag{5}$$

In the present experiments the above roughness parameters took the values of $\sigma = 0.09$ and $\mu = 0.31$ for the sparse configuration and $\sigma = 0.35$ and $\mu = 0.62$ for the dense configuration. For our particular configuration in which each element is equidistant to the surrounding ones, the parameters σ and μ are not independent, however this is not the case when the roughness elements are not equidistant from each other. The value of α was 0.5, 1 and 2.5 for each configuration. The above parameters can be combined to give the roughness frontal area per bed area parameter introduced by [18]

$$ah = \gamma\frac{dh}{\Delta S^2} = \gamma\alpha\mu^2 = \frac{4}{\pi}\alpha\sigma, \tag{6}$$

which varied between 0.06 and 1.13. An additional non-dimensional number associated with the flow's initial condition is

$$\lambda = \frac{h}{H}, \tag{7}$$

which is the ratio of the cylinder height to the water depth. In the present experiments λ varied between 0.03 and 0.5. Finally, the Froude and Reynolds numbers of the flow were defined as

$$Fr = \frac{U_f}{\sqrt{g'H}} \qquad \text{and} \qquad Re = \frac{U_f H}{\nu}, \tag{8}$$

where U_f is the front speed determined by linear interpolation of the $x{-}t$ coordinates of the $\rho' = 0.1$ contour at the leading front. In the present experiments the Froude and Reynolds numbers varied between $Fr = 0.15{-}0.47$ and $Re = 1100{-}22{,}000$. In order to determine the repeatability of each experiment and also the error associated with the determination of the front speed, we repeated one experiment four times with identical initial conditions. Both the Froude and Reynolds numbers were within 3% of the average value, confirming

that the methodology employed to perform the experiments and the determination of the front speed are robust.

4 Gravity current regimes

After the lock gate was removed the dense fluid in the lock created a dense gravity current which propagated through the regular field of roughness elements. Figure 2 shows the time averaged, non-dimensional 2D density field for a gravity current propagating over smooth, sparse and dense rough bottoms for different values of λ. Only the experiments having $\alpha = 2.5$ are shown, but similar density fields were obtained for all 35 experiments. The height of an energy-conserving current propagating over a smooth bottom is half of the lock height, i.e. $H/2$ [3]. We expect this scale to hold for a current propagating over a rough bottom with the difference that the current will be slightly higher to take into account the volume of the cylinders. When the current height was smaller than the roughness height, the current front had a triangular shape (Fig. 2 top row sparse and dense) similar to that observed for gravity currents propagating in a channel containing cylinders extending over the entire depth [29].

When the current height was larger than the roughness height, the gravity current propagated through the sparse and dense arrays of cylinders in two dynamically different regimes. Interesting, the qualitative behavior described below for the sparse and dense configurations shares some similarities with the flow in a two-layered porous media [11] although the Reynolds number is considerably larger in our study and the flow is governed by a different set of equations.

4.1 Sparse configuration

For a sparse configuration the dense current was observed to propagate between the cylinders. For $\lambda = 0.33$ (Fig. 2 middle column; second row) the current within the roughness elements maintained a triangular shape front and only a very small volume of the current was present above the obstacles. Hence, the current resembled again a current propagating in a channel with cylinders extending over the entire depth. However, for $\lambda \leq 0.25$ (Fig. 2 middle column; third, fourth and fifth row) there is clear evidence of two current fronts, one within and one above the obstacles, a behavior distinctively different from that observed when the cylinders extend over the entire depth. It is important to note that the front speed is the same for the part of the current traveling above and between the elements, in particular the two speeds are within 2% of the mean, i.e. speeds are identical within the experimental error. Mixing and entrainment were observed to be enhanced by the vortices generated in the wake of the cylindrical obstacles, as illustrated in the instantaneous non-dimensional density field of Fig. 3a. The density of the current head was substantially diluted by the entrainment of ambient fluid as indicated in the time averaged non-dimensional density fields by the region of reduced density in the middle column of Fig. 2 compared to the smooth bottom experiments illustrated in the left column.

For low values of λ (Fig. 2 middle column; fourth and fifth rows) the fraction of the current moving through the obstacles was either equal to or smaller than the fraction moving above the obstacles. Although the current front shape within the roughness elements, i.e. below the white line in Fig. 2, was still triangular, the entire front shape resembled that of a gravity current over a smooth bottom (Fig. 2 left column). The shape of

the current head approached that of a gravity current over a smooth bottom for the lowest values of λ (Fig. 2 middle column; last row), although the dilution was still significantly larger near the nose.

4.2 Dense configuration

For a dense configuration the current was observed to ride on top of the cylinders provided that the current height was larger than the obstacles' height, i.e. $\frac{H}{2h} > 1$ or equivalently, $\lambda < 0.5$ (Fig. 2 right column). The dense current above the cylinders and the ambient lighter water between the cylinders were observed to undergo convective instability as the dense water plunged vertically between the cylinders and displaced and mixed with the lighter water. This behavior is clearly illustrated in the instantaneous non-dimensional density field of Fig. 3b around $x' = 1.8$ where the current front above the cylinders is located above lighter fluid (blue). The density of the current head was significantly reduced by the mass exchange between the top dense fluid an the bottom light fluid and the dilution of the current head was enhanced for larger values of λ (Fig. 2 right column)

In most experiments, the highly dilute dense fluid produced between the cylinders by this process is observed to be almost stationary with negligible horizontal momentum, as verified by placing some potassium permanganate crystals in the fluid ahead of the current. Each of these crystals left a purple streak behind it as it fell down through the water column, acting as a passive tracer. Looking from the side of the tank, we observed that the purple streaks were almost motionless ahead of the dilute dense fluid between the cylinders, indicating that there was no motion. The 'apparent' current within the cylinders (Fig. 2 right column) is simply caused by this convective exchange and the current flux is almost entirely above the cylinders. In a few experiments, like the one shown in Fig. 2 (right column; second row), the dilute dense fluid produced between the cylinders was able to move slightly ahead of the front of the current propagating above the cylinders. The two different behaviors described above are observed to occur for different values of λ (Fig. 2 right column). In particular, for moderate and small values of λ, the dilute dense fluid between the cylinders is almost stationary and the front of the current riding on top of the obstacles is located, for small values of λ, above undiluted ambient water. For large values of λ, the diluted dense fluid between the cylinders moves such that it slightly leads the front of the current riding on top of the obstacles.

5 Gravity current dilution

For a dense configuration, the onset of convective instability allows for an efficient mechanism for mixing the dense gravity current whose dilution near the nose is, in general, greatly enhanced compared with both a gravity current in a sparse configuration and over a smooth bottom (Figs. 2, 3).

Figure 4 compares the time averaged non-dimensional vertical density profiles at different non-dimensional distances behind the current nose for dense, sparse and smooth configurations with $H = 20$ cm. For the sparse and dense configurations the cylinders' height was $h = 5$ cm, i.e. $\lambda = 0.25$. Near the nose of the current, $x' = -0.5$, the dilution is the largest both for the sparse and dense configurations. In the sparse configuration the density of the current between the cylinders decreases with height, while in the dense configuration the density is constant within the bottom roughness layer, indicating that

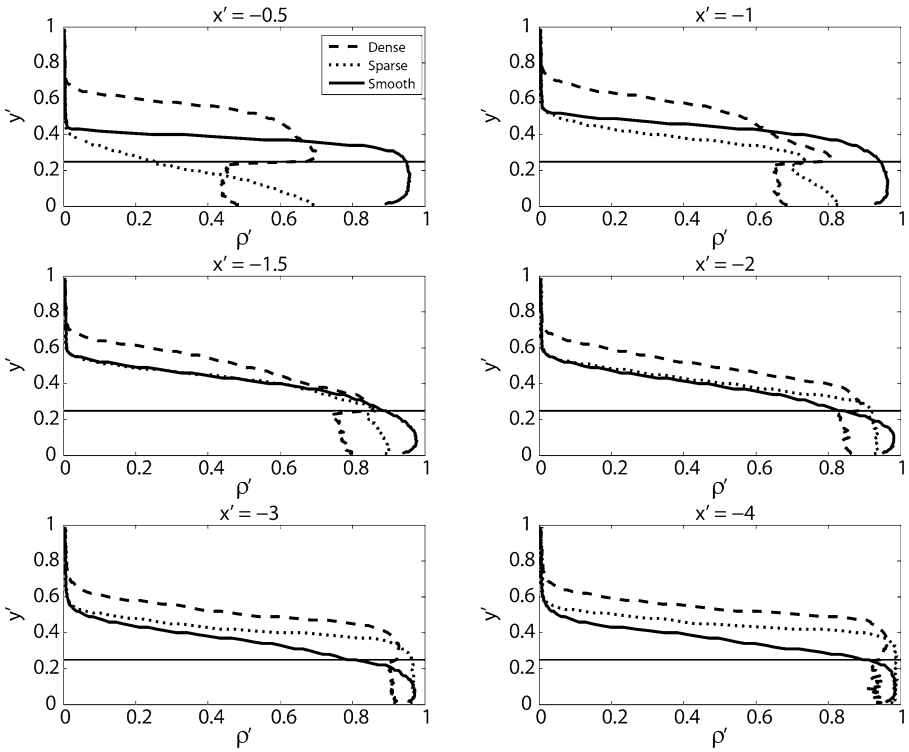

Fig. 4 Time averaged non-dimensional vertical density profiles for a gravity current propagating over a smooth bottom (*solid line*), and over a sparse (*dotted line*) and dense (*dashed line*) array of cylinders representing the bottom roughness. The non-dimensional parameters for the sparse and dense configuration experiments are the same as in Fig. 3 and for the smooth bottom experiment are: $\sigma = 0$, $\mu = 0$, $\alpha = 0$, $\lambda = 0$, $Fr = 0.46$ and $Re = 9313$. *Different panels* correspond to different locations behind the front as indicated above the panels by $x' = x/H$. *Thin black lines* indicate the height of the roughness elements for the sparse and dense configurations

convective instability is occurring and completely mixing the dense fluid with the ambient fluid. With increasing distance from the nose the difference in density between the smooth and the rough bottom cases diminishes. However, for $x' \leq -3$ the sparse configuration density maximum near the bottom is the same as for the smooth bottom, while for the dense configuration the density maximum near the bottom is still $\approx 10\%$ lower than for the smooth bottom and sparse configuration at $x' = -4$. For small x', i.e. far behind the current nose, the density profiles above the roughness elements are similar to those for a smooth bottom, albeit they are translated in the vertical since the gravity current height is larger due to the volume occupied by the cylinders.

6 Gravity current classifications

The two regimes, and the transition between them, can be characterized by two non-dimensional numbers: the ratio of the cylinder height to the lock height, λ, and the frontal area per bed area, ah. We classify all 30 experiments conducted with a rough bottom as a

function of the position of the nose of the dense current propagating on top of the cylinders relative to that of the front of the dense fluid between the cylinders. As illustrated in Fig. 5b, in one regime the dense fluid on the 'bottom' can propagate between the cylinders and lead the dense current on the top. This regime was observed mainly in the sparse configuration and, for a few experiments, in the dense configuration. In the second regime, the dense current propagates on the 'top' of the cylinders and the current front is ahead of the almost stationary dense fluid between the cylinders (Fig. 5c). This regime was observed only in the dense configuration. We will call these two regimes bottom and top, respectively, with the intent to indicate which fluid is leading.

The top regime is observed only for low values of λ, i.e. relatively deep currents, while the bottom regime is observed to occur mainly for large values of λ, i.e. relatively shallow currents. The transition between the top and bottom regimes (squares in Fig. 5a) is observed at higher values of λ for increasing values of ah. As shown in Fig. 5a by the dashed line, the top regime is observed approximately for $\lambda < 0.2ah$, the bottom regime approximately when $\lambda > 0.07 + 0.2ah$ (dashed-dotted line) and the transition occurred between $0.2ah \leq \lambda \leq 0.07 + 0.2ah$.

As expected, for low values of the parameters ah and λ the dense current behavior approaches that of a current over a smooth bottom. The black stars in Fig. 5a indicate both those experiments which have a smooth bottom-like behavior and the actual smooth bottom experiments occurring for $\lambda = 0$ and $ah = 0$. The largest deviations from the smooth bottom case are observed for large values of λ.

As discussed in Sect. 4.1, the speed of the current above and between the cylinders is identical within the experimental error, both in the top and bottom regime, i.e. Fig. 5b, c. This result is expected because the currents above and between the roughness elements are dynamically linked. In the bottom regime, the pressure head for the propagation of the current between the cylinders is given by the current flowing above the cylinders, while in the top regime, the bottom dense fluid is usually stationary and generated by the convective instability mixing dense fluid above the cylinders with the light fluid between the cylinders.

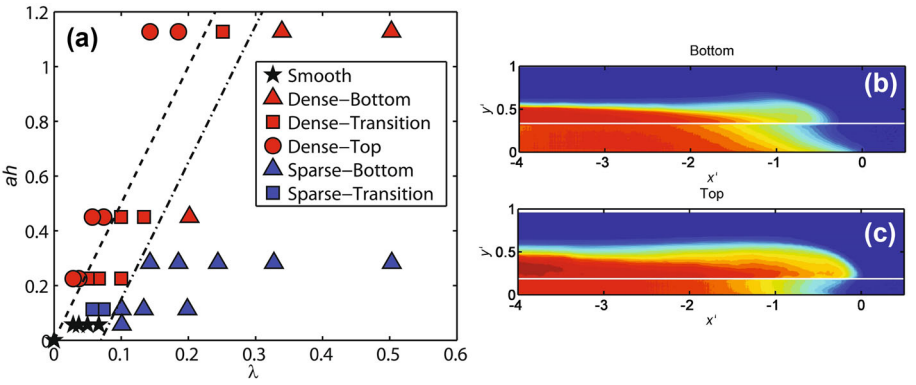

Fig. 5 **a** Classification of the different regimes as a function of the non-dimensional parameters λ and ah. *Dashed line* approximately marks the boundary of the top regimes region and its expression is given by $ah = 5\lambda$, while *dot-dashed line* marks the boundary of the bottom regimes region and its expression is given by $ah = 5\lambda - 0.35$. *Stars* indicate the smooth bottom experiments (i.e. five experiments overlaying at $\lambda = 0$ and $ah = 0$) and experiments in which the density field approached that of a gravity current over a smooth bottom. **b–c** Examples from Fig. 2 of time averaged non-dimensional density fields for gravity currents in the two regimes

In this regime, the location of the diluted dense fluid between the cylinders is dictated by the location of the current moving above the cylinders and the distance between the two fronts is constant in time.

7 Gravity current front speed

The front speed U_f is expected to decrease in the presence of a rough bottom due to the enhanced drag exerted by the cylinders. For a current propagating between the cylinders, the fraction of the current in contact with the cylinders decreases with increasing lock height, or equivalently, with decreasing cylinder height, both associated with a decrease in λ. Hence, the drag exerted by the cylinders has less impact on the front speed for smaller values of λ, resulting in a larger Froude number (Fig. 6).

When the current propagates on top of the cylinders, two different mechanisms are responsible for decreasing the Froude number as λ increases (Fig. 6). Both of these mechanisms are due to the convective instability between the dense current on top and the light fluid between the cylinders. Firstly, the mass exchange associated with this instability leads to the dilution of the current head and this dilution is enhanced as λ increases (Fig. 2 right column). A reduction of the head density reduces the dense current driving force and hence the Froude number. Secondly, the transfer of momentum between the dense current on top and the motionless light fluid between the cylinders has less impact on the front speed for smaller values of λ. In the above discussion, we have assumed that the convective exchange is largely independent of λ.

Furthermore, an increase in roughness density in general produced a decrease in the Froude number (Fig. 6). As the current switched from propagating between to propagating on top of the cylinders the two mechanisms due to convective instability described above

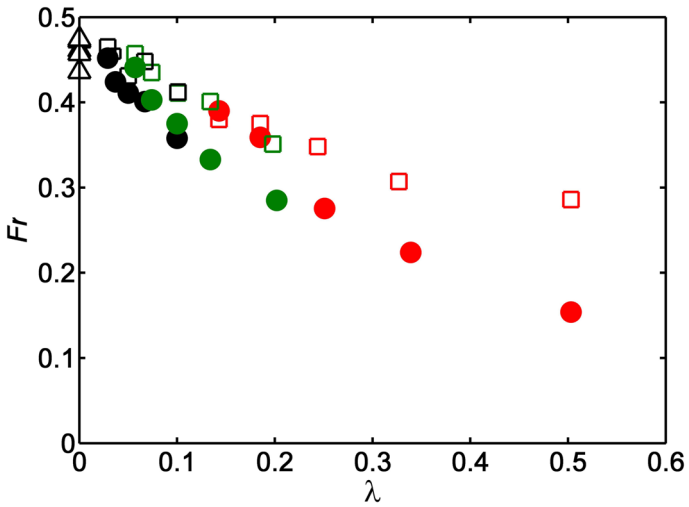

Fig. 6 Froude number dependence on λ for dense (*filled circles*) and sparse (*open squares*) configurations. *Red*, *green* and *black circles* or *squares* indicate cylinder heights of 5, 2 and 1 cm, respectively, while *open black triangles* indicate smooth bottom cases. The *error bars* correspond to the size of the symbols

are apparently more effective at reducing the Froude number than the form drag exerted by the cylinders.

For the smooth bottom currents the speeds for all experiments were within $5-10\%$ of the theoretical predicted value of $Fr = 0.5$ for an energy-conserving current which occupies half the depth of the channel [3], and have similar values to previous laboratory studies [26]. For low values of the depth ratio, i.e. for currents much higher than the cylinders and hence approaching the smooth bottom limit, the difference in Fr between the smooth and dense configurations is small and the Fr values converge towards the smooth bottom values 0.44-0.47. The difference between the Fr in the sparse and dense configuration increases with increasing λ as the dynamics of the two currents are different as described in Sect. 4.

An interesting result shown in Fig. 6 is that some of the experiments in the dense configuration present values of Fr close to, or in one case ($\lambda = 0.14$) larger than, the experiments in the sparse configuration having the same λ. This behavior can be explained as follows and is the focus of a companion study by Zhou et al. (pers. comm.). As discussed above, the Fr is expected to decrease when the dense current flows between the array of cylinders, i.e. $\sigma > 0$, compared to when it flows over a smooth bottom, i.e. $\sigma = 0$. However, in the limit of a very dense configuration, i.e. $\sigma \to 1$, the roughness covers the entire bottom and the current will be equivalent to that over a smooth bottom, with the slight difference that the initial fluid depth will be h less than that for the $\sigma = 0$ case. Hence, we expect that for large σ the Froude number will again increase, but to a lesser value than for $\sigma = 0$ due to the reduced depth caused by the roughness elements. Our results suggest that this behavior may be possible since for some experiments the dense current flowing on top of the cylinders (dense configuration) has a similar frontal speed, i.e. Fr, as the current having the same λ but flowing between the cylinders (sparse configuration).

8 Conclusions

We have investigated experimentally the dynamics regulating the entrainment and dilution of a lock-exchange dense gravity current flowing over a bottom roughness made of an array of vertical rigid cylinders.

For cylinders which are relatively far apart, i.e. sparse configuration, the dense current propagates between the cylinders and the front velocity is reduced when compared to a current flowing over a smooth bottom due to the enhanced drag exerted by the cylinders. The cylinders also generate vortices in their wakes which help homogenize the dense current. In addition, when the cylinder height is close to the dense current interface, the vortices in the wake are also able to enhance the dilution of the current by engulfing ambient water. This enhanced dilution is observed only behind the nose, while far away from the nose, i.e. $x' \leq -3$, the density is, in general, similar to that of a current over a smooth bottom.

When the cylinders are closer together, i.e. dense configuration, the dense current is unable to propagate between the cylinders given the large drag exerted by the rough bottom and instead is observed to propagate on top of the cylinders. This motion allows the dense water to be located above light water and the current therefore is subject to convective instability. The dense current dilution is effectively enhanced by this instability and its density is, in general, lower than for a current over a smooth bottom or in a sparse

configuration, at any location behind the nose. The details of this exchange mechanism will be the focus of a future contribution. We expect the volume of fluid exchanged between the current above and the fluid between the cylinders to decrease with increasing roughness density, and consequently the dilution of the current to be reduced. However, it is unclear if the mixing efficiency is going to be influenced by the roughness density when convective instability occurs.

Finally, the front of the current riding on top of the obstacles is ahead of the almost stationary less dense fluid between the cylinders for $\lambda < 0.2ah$, while the dense fluid between the cylinders propagates and leads the dense current on the top for $\lambda > 0.07 + 0.2ah$. Hence, given the parameters λ and ah, or the equivalent non-dimensional numbers introduced in Sect. 3, convective instability should occur for $\lambda < 0.2ah$ leading to enhanced dilution.

Acknowledgements The authors would like to thank Ian Sheppard and Kevin Wines for their invaluable technical expertise in constructing the experimental apparatus at the University of Canterbury. Support to C.C. was given by the National Science Foundation Project OCE-1333174. Support to J.H. was provided by the MMA Travel Fund.

References

1. Adduce C, Sciortino G, Proietti S (2011) Gravity currents produced by lock exchanges: experiments and simulations with a two-layer shallow-water model with entrainment. J Hydraul Eng 138(2):111–121
2. Belcher SE, Harman IN, Finnigan JJ (2012) The wind in the willows: flows in forest canopies in complex terrain. Annu Rev Fluid Mechan 44:479–504
3. Benjamin TB (1968) Gravity currents and related phenomena. J Fluid Mech 31(02):209–248
4. Britter R, Hanna S (2003) Flow and dispersion in urban areas. Annu Rev Fluid Mech 35(1):469–496
5. Cantero MI, Lee J, Balachandar S, Garcia MH (2007) On the front velocity of gravity currents. J Fluid Mech 586:1–39
6. Cenedese C, Adduce C (2010) A new parameterization for entrainment in overflows. J Phys Oceanogr 40(8):1835–1850
7. Cenedese C, Dalziel SB (1998) Concentration and depth fields determined by the light transmitted through a dyed solution. Proceedings of the 8th International Symposium on Flow Visualization, p 8
8. Finnigan J (2000) Turbulence in plant canopies. Annu Rev Fluid Mech 32(1):519–571
9. Hacker J, Linden P, Dalziel S (1996) Mixing in lock-release gravity currents. Dyn Atmos Oceans 24(1):183–195
10. Hallberg RW (2000) Time integration of diapycnal diffusion and richardson number-dependent mixing in isopycnal coordinate ocean models. Mon Weather Rev 128(5):1402–1419
11. Huppert HE, Neufeld JA, Strandkvist C (2013) The competition between gravity and flow focusing in two-layered porous media. J Fluid Mech 720:5–14
12. Huppert HE, Simpson JE (1980) The slumping of gravity currents. J Fluid Mech 99(04):785–799
13. Huq P, White LA, Carrillo A, Redondo J, Dharmavaram S, Hanna SR (2007) The shear layer above and in urban canopies. J Appl Meteorol Climatol 46(3):368–376
14. Jackson LR, Hallberg RW, Legg S (2008) A parameterization of shear-driven turbulence for ocean climate models. J Phys Oceanogr 38(5):1033–1053
15. La Rocca M, Adduce C, Sciortino G, Pinzon AB (2008) Experimental and numerical simulation of three-dimensional gravity currents on smooth and rough bottom. Phys Fluids 20(10):106603 (1994-present)
16. Necker F, Härtel C, Kleiser L, Meiburg E (2005) Mixing and dissipation in particle-driven gravity currents. J Fluid Mech 545:339–372
17. Negretti ME, Zhu DZ, Jirka GH (2008) The effect of bottom roughness in two-layer flows down a slope. Dyn Atmos Oceans 45(1):46–68
18. Nepf HM (2012) Flow and transport in regions with aquatic vegetation. Ann Rev Fluid Mech 44:123–142
19. Nogueira HI, Adduce C, Alves E, Franca MJ (2013) Analysis of lock-exchange gravity currents over smooth and rough beds. J Hydraul Res 51(4):417–431

20. Nogueira HI, Adduce C, Alves E, Franca MJ (2014) Dynamics of the head of gravity currents. Environ Fluid Mech 14(2):519–540
21. Nokes R (2016) Streams 2.05—system theory and design. University of Canterbury, Christchurch
22. Ooi SK, Constantinescu G, Weber L (2009) Numerical simulations of lock-exchange compositional gravity current. J Fluid Mech 635:361–388
23. Ozan AY, Constantinescu G, Hogg AJ (2015) Lock-exchange gravity currents propagating in a channel containing an array of obstacles. J Fluid Mech 765:544–575
24. Özgökmen TM, Iliescu T, Fischer PF (2009) Large eddy simulation of stratified mixing in a three-dimensional lock-exchange system. Ocean Modelling 26(3):134–155
25. Rottman JW, Simpson JE (1983) Gravity currents produced by instantaneous releases of a heavy fluid in a rectangular channel. Journal of Fluid Mechanics 135:95–110
26. Shin JO, Dalziel SB, Linden PF (2004) Gravity currents produced by lock exchange. J. Fluid Mech. 521:1–34
27. Simpson JE (1997) Gravity currents in the environment and the laboratory. Cambridge University Press, Cambridge
28. Tanino Y, Nepf HM (2008) Laboratory investigation of mean drag in a random array of rigid, emergent cylinders. J Hydraul Eng 134(1):34–41
29. Tanino Y, Nepf HM, Kulis PS (2005) Gravity currents in aquatic canopies. Water Resour Res 41(12):W12402
30. Testik FY, Yilmaz N (2015) Anatomy and propagation dynamics of continuous-flux release bottom gravity currents through emergent aquatic vegetation. Phys Fluids 27(5):056603 (1994-present)
31. Ungarish M (2009) An introduction to gravity currents and intrusions. CRC Press, Boca Raton
32. Xu X, Chang YS, Peters H, Özgökmen TM, Chassignet EP (2006) Parameterization of gravity current entrainment for ocean circulation models using a high-order 3d nonhydrostatic spectral element model. Ocean Model 14(1):19–44
33. Zhang X, Nepf HM (2008) Density-driven exchange flow between open water and an aquatic canopy. Water Resour Res 44(8):W08417
34. Zhang X, Nepf HM (2011) Exchange flow between open water and floating vegetation. Environ Fluid Mech 11(5):531–546